Super-Resolution in Magnetic Resonance Imaging: A Review

ERIC VAN REETH,[1] IVAN W. K. THAM,[2] CHER HENG TAN,[3] CHUEH LOO POH[1]

[1] *School of Chemical and Bioengineering, Nanyang Technological University, Singapore*
[2] *Department of Radiation Oncology, National University Cancer Institute, Singapore*
[3] *Department of Diagnostic Radiology, Tan Tock Seng Hospital, Singapore*

ABSTRACT: For the last 15 years, super-resolution (SR) algorithms have successfully been applied to magnetic resonance imaging (MRI) data to increase the spatial resolution of scans after acquisition has been performed, thus facilitating the doctors' diagnosis. The variety of application and techniques has grown ever since, especially in the MRI modality, showing the interest of the community to such postacquisition processing. This article presents a review of the general principle of SR as well as how this principle has been adapted to MRI data. The main algorithms and the principal acquisition protocols are detailed for both static and moving subjects. The presented strategies are discussed and compared according to the data specificities. Later, different ways of measuring the resolution enhancement and quantify the benefit of SR are detailed. Finally, unexplored perspectives on the application of SR to MRI data are discussed. © 2012 Wiley Periodicals, Inc. Concepts Magn Reson Part A 40A: 306–325, 2012.

KEY WORDS: medical imaging; super-resolution; MRI; interpolation; volume reconstruction

I. INTRODUCTION

Magnetic resonance imaging (MRI) is today widely used to assess brain disease, spinal disorder, angiography, cardiac function, and musculoskeletal damage. Although MRI requires a larger acquisition time than computed tomography (CT), MRI does not require the use of ionizing radiation and scans can be performed at any chosen orientation. It features full three-dimensional (3-D) capabilities, excellent soft-tissue contrast and high spatial resolution. Furthermore, MRI allows functional, diffusion and perfusion imaging to be performed.

In many medical applications, high-resolution 3-D images are required to facilitate early and accurate diagnosis. However, due to acquisition constraints such as limited acquisition time or moving subjects, a sufficient sampling density cannot always be reached. Image processing techniques can be applied to increase the image resolution a posteriori. In most MRI machines, a basic interpolation (usually zero-padding) is available
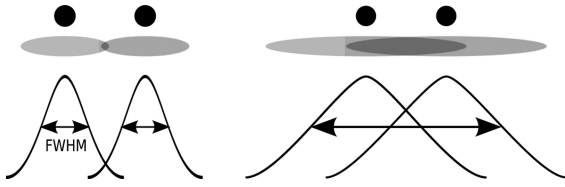
Figure 1 Left: The two point sources can be resolved because the FWHM of the PSF is smaller than the point sources separation. Right: The two points cannot be resolved.

to increase the size of the images. Applying this interpolation facilitates the visualization but several artifacts such as blur and contrast loss are added, while no new information is introduced into the image. Super-resolution (SR) techniques offer the possibility to efficiently improve the resolution of scans, ensuring the addition of significant new information and increasing the diagnosis possibilities.

Potential Clinical Applications

Currently available clinical MRI systems are able to provide sub-centimeter resolution for static scans. However, small but clinically significant lesions in joints, brain or pelvis may still be challenging to correctly visualize or characterize. Some tumors, such as nasopharyngeal carcinoma, demonstrate a high rate of perineural invasion, which can appear subtle even for MRI. MRI-detected cranial nerve involvement has been shown to be an adverse prognostic factor in nasopharyngeal carcinoma (*1*), and improving imaging resolution could improve the sensitivity for the detection of this important factor and guide delivery of appropriate radiation doses for treatment.

The increasing use of functional imaging to interrogate intratumoral heterogeneity has led to a clinical need for improved spatial resolution for inherently low-resolution sequences. Due to the technical ability to deliver dissimilar radiation doses to different subvolumes within the tumor target (also termed dose-painting), there is a clinical need to accurately determine the regions that may be relatively radio-resistant and hence require a higher dose to achieve adequate tumor cell kill (*2*).

The development of whole body MRI, with (*3*) or without hybrid positron emission tomography (*4*), as well as the imaging of moving organs such as heart ventricles and upper abdominal visceral organs, has also increased the requirement for high spatial and temporal resolution imaging. The application of SR in this setting could allow more rapid through-put or more sequences within a reasonably tolerable time frame.

Spatial Resolution Limitations

Strictly speaking, spatial resolution is defined as the smallest separation of two point sources necessary for the source to be resolved. The mathematical relationship between the acquired image $I(x, y, z)$ and the physical object $O(x, y, z)$ being imaged can be represented by:

$$I(x, y, z) = O(x, y, z) \star h(x, y, z) \qquad [1]$$

where $\star$ represents the convolution operator and $h(x, y, z)$ is the 3D point spread function (PSF). Figure 1 illustrates the relationship between image resolution and PSF. It shows that two point sources can be resolved, if they are separated by a distance greater than the full width at half maximum (FWHM) of the PSF.

In MRI, the PSF is usually anisotropic, because the acquisition process is different for each dimension. The dimension convention used throughout this article is presented in Fig. 2. The phase-encoding and frequency-encoding dimensions are referred as the in-plane dimensions, and the slice-select (or through-plane) dimension is referred as through-plane dimension. The slice-select resolution is strictly linked to the frequency response of the slice-selective RF pulse. The PSF in the frequency and phase encoding directions is mainly affected by three factors: the digital resolution, data truncation, and relaxation during acquisition (*5*):

- The digital resolution is obtained by dividing the field of view (FOV) by the number of data points acquired in each dimension.
- Data truncation occurs, because only a finite number of data points can be acquired. The width of the PSF is then inversely proportional to the number of samples acquired in the corresponding dimension.
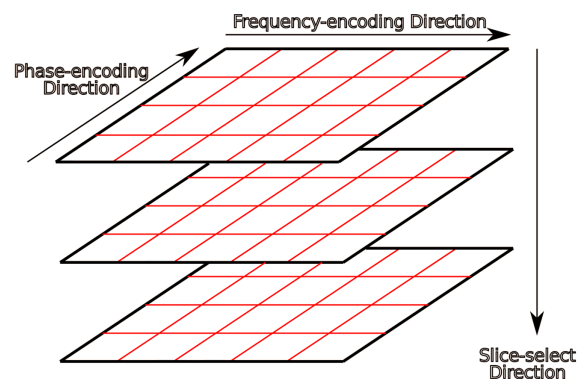

Figure 2 Illustration of the dimension convention for a multislice MRI scan.

- The final factor is the degree of T_2^* relaxation during data acquisition. The higher the degree of T_2^* relaxation the narrower the PSF.

For an optimal representation of a 3D volume, a 3-D Dirac delta function PSF is desired, but this theoretical limit is not reachable in practice. This would require the application of an infinite RF pulse to increase the selectivity of the slice selection process and the acquisition of an infinite number of data points. This would result in a dramatic increase in the overall acquisition time, which would fall beyond the limit of a realistic practical application.

Another factor that limits the spatial resolution during the acquisition is the presence of moving subjects. In these situations, typically cardiac imaging, fetal MRI, functional MRI, or uncooperative patients, scanning times are required to be extremely fast to avoid motion artifacts. Such speeds can be reached by using gradient-echo sequences (such as FLASH, FISP, SSFP, and GRASS) in addition to the reduction of the in-plane resolution and larger slice thickness. Consequently, high-resolution images can seldom be acquired in the presence of motion, justifying the growing interest for postacquisition resolution improvement methods.

Increasing the Resolution of MR Images

Several approaches can be used to increase the overall resolution of MRI scans. Hardware improvements directly increase the resolution of the acquired images. For example, increasing the number of coil receiver channels or increasing the main magnetic field going through the MRI core, B_0 increases the MRI signal. For a similar SNR value, scanners with a high value of B_0 and a high number of coil receiver channels will produce images with higher spatial resolution and contrast (*6*). Nowadays, most MRI scanners used for medical purposes have B_0 values of 1.5 or 3 T and can reach typical resolutions of around $1.5 \times 1.5 \times 4$ mm^3. In parallel, ultra-high magnetic field MRI scanners with $B_0 = 11.7$ T are developed for research purpose and resolutions of $80 \times 80 \times 200$ μm^3 have been reported (*7*).

Independently from any hardware improvement, postacquisition image processing techniques such as SR can also be applied to increase the resolution of MR images. They present the advantage to be applicable on all MRI machines and in many practical situations, without requiring the purchase of new hardware equipments. The main advantage of SR methods is to offer the possibility to reconstruct high-SNR and high-resolution representations of objects that could only be acquired at low resolution because of subject motion, scanning time limitation, or SNR considerations.

Introducing the SR Technique

SR algorithms have first been introduced in the early 1980s and were applied to video processing to increase the resolution of image sequences (*8–11*). The idea behind SR is to combine several distinct low-resolution observations of the same object to reconstruct a high-resolution image. In video sequences, a high-resolution frame at time t_0 can be created from consecutive frames containing the same object if this object has moved by a subpixel amount as illustrated in Fig. 3 for a simple translation. When the geometric transformation (translation, rotation, and deformation) of the objects along the frames is known or correctly estimated with subpixel accuracy, it is possible to combine low-resolution images into a high-resolution image that contains additional frequency content. Retrieving aliased content is a major advantage for SR over standard interpolation techniques.

The MRI framework is particularly well adapted to the application of SR techniques because of the control one has over the acquisition process. In particular, as any scanning plane orientation can be chosen, several distinct low-resolution observations of the subjects can be acquired even when no subject motion is involved. Moreover, the resolution of MRI images is often limited by several factors such as SNR limitations, moving subjects, and limited scanning times. In such cases, images with large slice thickness and low in-plane resolution are generally acquired which provides a good basis for SR algorithms to succeed and overcome the missing of critical information when the Nyquist sampling criterion is not met, that is, when aliasing is present in the acquired image. Several authors have demonstrated the benefit of using SR reconstruction methods compared to direct high-resolution acquisition. They showed that for a given acquisition time the SR reconstructed images presented higher SNR when compared to images directly acquired at the same resolution (*12, 13*). This is of great interest for practical applications, because it offers the possibility to decrease the acquisition time, which is often a critical parameter, and reconstruct the high-resolution image a posteriori.

The application of SR to MRI was first reported in Ref. *14* in 1997. Since then, a large number of articles adapting the SR concept from video processing to multidimensional MRI data have been reported, and encouraging results have been demonstrated. Several acquisition protocols have been introduced and successfully applied on both static and moving subjects,
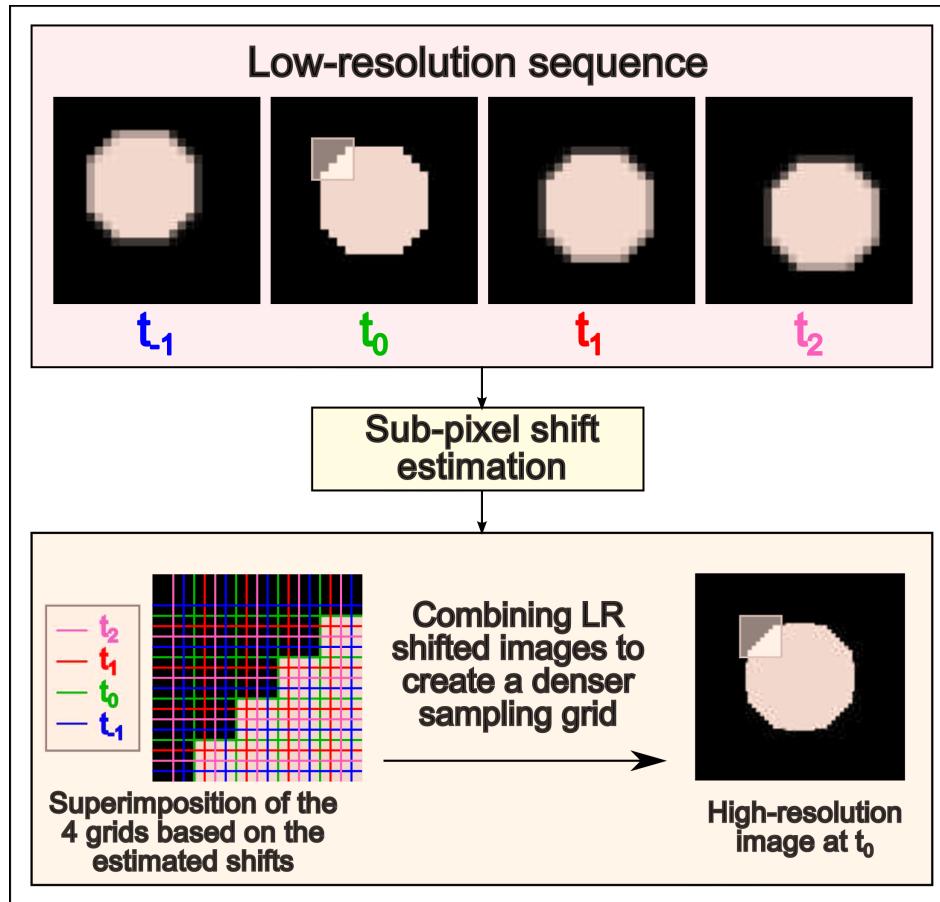
Figure 3 Introducing the SR principle.

and numerous algorithms have been developed and optimized to fit the MRI data specificities.

Structure and Objective of the Article

SR in the context of MRI and PET has been presented in a previous review by Greenspan et al. (*15*). In the MRI part of the article, the authors discuss the dimensionality of the SR problem and give an overview of the various algorithms and the application of SR to static MRI subjects using parallel acquisitions. Our article extends the previous review by presenting multiorientation acquisition protocols to perform SR on static subjects. It also studies and reviews the application of SR in the context of moving subjects, which has been a subject of growing interest in recent years, and provides the reader with different methodologies to assess and measure the resolution enhancement. Additionally, this article discusses the choice of the SR method to guide the novice reader toward the optimal solution.

In the first part of this article, the feasibility of SR in both in-plane and through-plane dimensions is discussed. Necessary conditions for in-plane resolution

enhancement has been a subject of many discussions in the past and the latest arguments are presented. Then Section III studies the specificity of MRI data to adapt the general SR observation model to the MRI case. The different SR algorithms are then presented and compared in section "SR Algorithms". Later, Sections IV and V provide an overview of acquisition protocols required for SR to succeed, respectively, in the presence of static and moving subjects. Finally, different ways of measuring the improvement of resolution are discussed in Section VI, and section VII provides some promising and up-to-date perspectives still to be explored.

II. FEASIBILITY OF SR IN MRI

In video applications, SR algorithms use the motion between successive frames to create additional information. In MRI scans, motion does not occur when static subjects are scanned: brain MRI, bone MRI, and so forth. Resolution improvement in these situations can, however, be reached by acquiring several sub-pixel shifted scans of the same subject. This section

discusses the feasibility of SR both for the in-plane and for through-plane dimensions and the necessary conditions that apply on the shifts performed.

In-Plane Improvement

The anisotropy of the voxels of multislice MRI scans have encouraged the majority of authors to apply SR algorithms to enhance the through-plane resolution. However, some articles have also studied in-plane resolution improvement (*16, 17*). To achieve in-plane resolution improvement, several scans with subpixel shifted FOV in the in-plane directions were acquired. SR was applied to produce a high-resolution image, which showed a clear resolution improvement in the in-plane dimension, and higher SNR.

However, questions were raised in Refs. *18*, *19*, *20* about the theoretical nature of the in-plane resolution improvement shown in Ref. *16*. MRI data are acquired in the Fourier-encoded frequency domain (*k*-space). Consequently, spatial subpixel FOV shifts in the in-plane dimension correspond to a linear phase modulation in the *k*-space, if the FOV and the digital resolution remain the same throughout the scans. Under these conditions, the *k*-space points acquired are identical for all the scans, and no new frequency content is acquired. Scheffler (*18*) stated that similar results could be obtained by combining the same number of scans without introducing any shifts. In Ref. *19*, the authors demonstrated that similar in-plane resolution improvement can be replicated using zero-padding interpolation. According to them, the improvement in resolution would only be due to noise reduction that resulted in a SNR improvement.

However, in a separate study (*17*), Tieng et al. have combined images that were initially acquired at the same sample points in the *k*-space domain but shifted numerically afterward. The result of this combination was compared to the reconstruction obtained from the same number of images but acquired with shifted FOVs. Results comparison clearly showed that the shifted FOVs images contain more high frequencies, suggesting that new information was indeed introduced when FOVs were shifted. According to them, shifting the FOV by changing the demodulation frequency of the receiver produce low-resolution images that contain exclusive frequency content.

Although both parties have not converged yet toward a common view, some points about improving the in-plane resolution remain clear:

- Combining in-plane FOV shifted images does improve SNR, which leads to image quality enhancement especially in the case of noisy data.

- Because only a finite number of in-plane data samples can be acquired, the in-plane data is inherently band-limited. This limits the potential overall in-plane resolution improvement.
- If the object is shifted before the acquisition, new information (although a very small amount) is added when several low-resolution images are combined (*21*).

In addition, some articles have demonstrated in-plane resolution improvements under specific conditions. It has been proven in Ref. *22* that using spatially shifted scans performed at different FOVs does improve in-plane resolution (although experimental results are not satisfying). In Ref. *23*, in-plane resolution enhancement was performed in the case of parallel MRI. Images were acquired at the same FOV and resolution, but the authors showed that complementary information of the subject, as they come from different receiver channels.

Through-Plane Improvement

As discussed in the previous paragraph, the in-plane resolution of multislice scans is much higher than the through-plane resolution. This explains why most articles have proposed SR methods to decrease the slice thickness and reach voxel isotropy. Unlike in the in-plane dimension, the sampling rate in the through-plane dimension is usually too low, which causes the slice selection process to create aliasing. This provides a good basis for SR algorithms to efficiently reconstruct high-frequency content in this dimension.

Following the same idea introduced for in-plane resolution improvement, several low-resolution volumes are acquired with the introduction of a known subpixel shift between them. Various acquisition schemes have been proposed to optimize the enhancement of the slice-select dimension. They will be detailed in section IV.

III. GENERAL MODEL AND ALGORITHMS

Each SR algorithm relies on an acquisition model. Parameters of this model are fundamental, as the high-resolution image estimation is optimized toward it. A well-established general form of this model can be given without any loss of generality on the dimensionality of the problem (*24*). Let $\{Y_k\}_{k=1}^{N}$ be a set of low-resolution observations obtained from the following imaging model illustrated in Fig. 4:

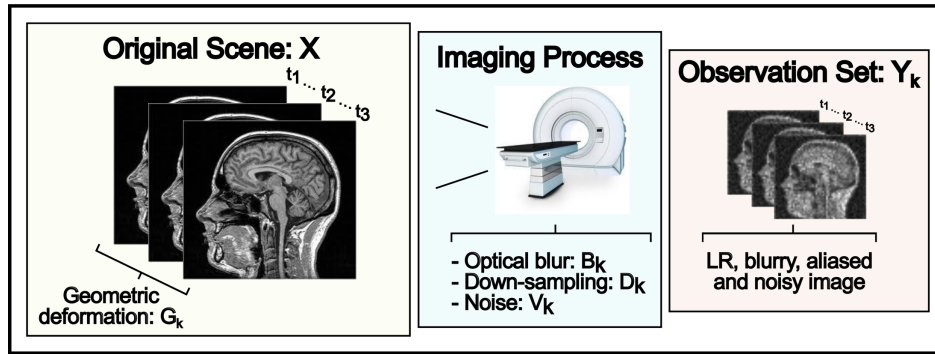$$Y_k = D_k B_k G_k X + V_k, \quad k = \{1, \ldots, N\} \quad [2]$$

Figure 4   The general acquisition model.

where X is the high-resolution image given at an arbitrary reference position k_r, G_k is the geometric transformation from the image Y_k to the reference image Y_{k_r}, B_k is the space-variant blur operator modeling the PSF of the imaging process, D_k is the down-sampling operator, and V_k is an additive zero mean Gaussian noise. The SR process aims at inverting the given model to find the original non-noisy, nonblurry, high-resolution image. Because the inversion of such a problem is ill-posed, optimization methods will be employed to estimate the best solution given the acquisition parameters and the low-resolution observations.

Without loss of generality, the model in Eq. [2] can be written as:

$$Y_k = W_k X + V_k, \quad k = \{1, \ldots, N\} \qquad [3]$$

where W_k is the global transformation operator that includes geometric transformation, blur and down-sampling from the high resolution to the low-resolution image.

Note that an additive model has been proposed in Ref. *25* to represent the relation between the high-resolution and the low-resolution volumes.

Adapting the Model to MRI Data

In the context of video processing, several types of blur, noise models, and down-sampling operators have been studied. This section reviews the choice of different operators in the context of MRI data.

Geometric Transformation.   The operator G_k represents the geometric deformation between the kth frame and the k_rth reference frame. Geometric deformation (often called warping or motion) is fundamental in the SR process, because it provides different views of the same object, bringing in additional information. The deformation has to be of subpixel nature to provide additional information, which requires a very accurate

deformation estimation. Such a precision is sometimes difficult to guarantee in practice, and this often makes registration a bottleneck in the SR process. For this reason, predetermined motion is often introduced to improve the quality of the high-resolution reconstruction. In SR applications involving static subjects, the motion is artificially created by shifting or rotating the scan FOV by a known value. Such acquisition protocols have been widely used and are detailed in Section IV.

However, when the subject itself is moving or deforming, no FOV shifts are theoretically required to apply SR, and registration has to be performed. Generally, it has been shown that due to registration errors, the presence of unknown motion decreases the potential resolution enhancement. In practice, predetermined shifts are also introduced to optimize the efficiency of the k-space sampling. Such protocols will be reviewed in Section V.

Modeling the PSF.   The operator B_k represents the amount of blur added during the overall acquisition process and is often assimilated to the blur introduced by the imaging system. It is commonly assumed that the PSF induced by the MRI acquisition process is space-invariant, which simplifies B_k into B. Although B is a 2D operator in most video applications, a third dimension is added to take into account the slice-select dimension of 3D MRI stacks. In Ref. *26*, the authors have compared the effect of using different shapes of PSF to conclude that 3D anisotropic PSF lead to the best results. In most medical applications, the PSF in the slice-select dimension is defined as the slice excitation profile.

Most articles dealing with MRI SR suggest that the PSF is well approximated by a Gaussian function in the three dimensions (*5, 19, 22, 26–30*). It is commonly assumed that in the slice-select dimension, the FWHM of the PSF should be equal to the slice thickness of the MRI volume. Moon and Harnak (*31*) have proposed a

MRI-compatible phantom that can be used to measure the in-plane PSF.

Alternative models of blurring have also been proposed. Poot et al. (*32*) have regrouped the blur step and the down-sampling step. They proposed to use a 3D separable sampling function instead of a Gaussian function as a representation of the digitalization process. Rectangular PSF, or box-PSF, which approximates the slice-select profile by a constant throughout the slice thickness, has also been studied in Ref. *19*.

Down-Sampling Operator. The down-sampling operator is usually directly deduced from the dimensions of the required high-resolution volume, except in the case where slice-spacing is non-null. A solution was proposed in Ref. *33* where a model of the slice-select acquisition was introduced and coupled with an in-painting SR algorithm.

SR Algorithms

The general model given in Eq. [2] can be solved using different approaches. A complete overview of such algorithms is given in Ref. *34*, but this section reviews the ones that have been used on MRI data so far. The choice of which SR algorithm to use is discussed in Section "Choice of SR Method".

Back-Projection Approach. Iterative back-projection (IBP) algorithms were introduced by Irani and Peleg (*9, 11, 35*). This approach is based on the previously defined imaging model of Eq. [2]. A first high-resolution estimation is performed, $\hat{X}$, and the imaging process is applied to obtain a set of low-resolution images $\hat{Y}_k$ that corresponds to the simulation of the real observed images Y_k. An iterative process is introduced to minimize the following error function:

$$\epsilon^{(n)} = \sqrt{\sum_{k=1}^{N} \left(Y_k - \hat{Y}_k^{(n)}\right)^2} \qquad [4]$$

where n is the current estimation and N the total number of observations. The current estimation is updated by the following procedure:

$$\hat{X}^{(n+1)}(x) = \hat{X}^{(n)}(x) + \sum_{y \in \cup_k \Delta_{k,x}} \left(Y_k(y) - \hat{Y}_k^{(n)}(y)\right) \times h_{xy}^{BP} \qquad [5]$$

where y and x denotes, respectively, low-resolution and high-resolution pixels, h^{BP} is the back-projection kernel, and Δ_{kx} is the set $\{y \in Y_k \mid y$ is influenced by $x\}$. The back-projection kernel weights the contribution of

the low-resolution pixels y to update the current estimation. Different choices of h^{BP} are discussed Ref. *11*, in which the authors point out that $h^{BP} = h^{PSF}$ is generally a good choice regarding stability and noise addition.

In practice, there are several possible solutions to this problem between which the algorithm might oscillate. The initialization has no influence on the stability and on the speed of the convergence but might influence the solution that is reached first. Irani and Peleg (*11*) recommend the average image of low-resolution images as a reasonable initial guess.

This method has been used in MRI SR because of its simplicity (*16, 26, 33, 36*). However, due to the ill-posed nature of the inverse problem, the solution reached might not be unique. To overcome this issue, prior knowledge about the solution can be introduced to stabilize the inversion of the equation. Such approaches, referred as regularized approaches, are covered in the next section.

Deterministic Regularized Approach. Using a priori information about the solution can turn the model described previously in Eq. [3] into a well-posed problem. Typically a smoothness constraint is applied on the solution, to limit the apparition of unexpected high-frequencies, focusing on the restoration of the low-frequency contents of the image. In the case of a constrained least-square regularization, the optimal solution X minimizes the following Lagrangian:

$$\hat{X}_R = \text{argmin} \left[\sum_{k=1}^{N} ||Y_k - W_k \hat{X}||^2 + \gamma ||C\hat{X}||^2\right] \qquad [6]$$

The notations of Eq. [3] are used, C represents a high-pass filter, and γ is called the Lagrange multiplier or regularization parameter. It balances the trade-off between the data fidelity term and the a priori knowledge term. Considering the problem as a convex optimization, gradient descent algorithms can be applied to converge toward the optimal solution. The iterative scheme can then be written as:

$$\hat{X}_R^{n+1} = \hat{X}_R^n + \beta \left(\sum_{k=1}^{N} W_k^T (Y_k - W_k \hat{X}_R^n) - \gamma C^T C \hat{X}_R^n\right) \qquad [7]$$

where β is the step size in the gradient direction. If the chosen regularization term is a convex function, this equation converges toward a unique solution. The choice of C as a high-pass filter leads inexorably to edge alterations in the final solution, which is why alternative regularizers have been studied in the context of MRI

to preserve the frequency content of the reconstructed image.

In Ref. *25*, the regularization term consists of minimizing the first derivative of the image in the through-plane dimension, using a Hubert function (quadratic function). In a related approach, Poot et al. (*32*) minimize the sum of the square of the second derivative of the reconstructed image. In Ref. *37*, the regularization is based on the total variation operator, which was introduced in Ref. *38*, and which is often used for its denoising and edge preserving properties. In Ref. *39*, two regularization terms were used. The first one is a directional version of the total variation constraint (DBTV), and the second one, the Tri-modal regularizer, is designed to benefit from a priori knowledge on intensities of brain MRI. In Ref. *40*, SR is applied on diffusion brain MRI to detect fiber orientation and volume fraction. The quadratic regularization terms are defined according to a physical model and penalize high differences in volume fractions of neighboring voxels, while favoring the anisotropy in the fibre orientations of neighboring voxels.

An interesting approach is described in Ref. *41*, where nonlocal regularizers are used, in contrast to pixel-based approaches. Nonlocal methods model the many regularities and geometries seen in local patterns of training data or input images to develop explicit models. The same authors in Ref. *42* introduced another nonlocal regularizer to enhance the resolution of a T_2-weighted MRI volume. The intermodality regularizer uses prior knowledge from a reference high-resolution T_1-weighted volume of the same subject, to constrain the reconstruction of the high-resolution T_2-weighted volume into a realistic solution.

Statistical Regularized Approach. Stochastic regularization is more flexible to include a priori knowledge than deterministic models. Bayesian estimation methods are used when the a posteriori probability density function (PDF) of the original image can be established. The maximum likelihood (ML) estimator of the high-resolution volume X_{ML} maximizes the a posteriori PDF: $P(X|Y_k)$ with respect to X, based on the observations Y_k.

$$X_{\mathrm{ML}} = \mathrm{argmax}\,[P(X|Y_k)] \qquad [8]$$

ML estimators have been used on MRI brain data in Ref. *43*, to reconstruct volumetric images from multiple-scan slice acquisitions.

Prior knowledge on X can be included to the model by applying Bayes theorem to Eq. [8]. This model is referred as the maximum a posteriori (MAP) method. It follows from Eq. [9] that X_{MAP} can be expressed as a sum of the likelihood term and the prior term:

$$X_{\mathrm{MAP}} = \mathrm{argmax}\,[\ln(P(Y_k|X)) + \ln(P(X))] \qquad [9]$$

As $P(X)$ represents a priori constraints on X, it plays the role of regularizer. Various image priors can be used to estimate $P(X)$. Markov random field (MRF) priors that provide a powerful method for image prior modeling are adopted in Refs. *44*, *45*, *46*. The potential function of the MRF usually depends on the derivatives of the image that evaluates the cost caused by the irregularities of the solution. Gholipour et al. (*29, 30*) presented a simpler expression of $P(X)$ that involves a quadratic exponential function such as:

$$P(X) = \exp(-X^{\mathrm{T}}QX) \qquad [10]$$

where $Q = C^T C$, and C is the gradient magnitude operator.

Finally, to model the likelihood term of Eq. [9], $P(Y_k|X)$, a Gaussian distribution with zero mean and standard deviation of σ_k is often used to represent the noise residual (error samples).

$$P(Y_k|X) = \prod_i \frac{1}{\sigma_k\sqrt{2\pi}} \exp\left(-\frac{(\hat{Y}_k(i) - Y_k(i))^2}{2\sigma_k^2}\right)$$
$$[11]$$

Estimated observation samples $\hat{Y}_k$ are obtained based on $\hat{X}$ by reversing the observation model of Eq. [2]. If the error between frames is assumed to be independent, the optimization problem can be expressed more compactly as:

$$\hat{X}_{\mathrm{MAP}} = \mathrm{argmin}\left[\sum_{k=1}^{N} ||Y_k - W_k\hat{X}||^2 + \gamma\Phi(\hat{X})\right]$$
$$[12]$$

where γ is the weighting regularization parameter, and Φ is the function that expresses the prior term $P(X)$. In this configuration, the data fidelity term of Eq. [12] is similar to the one of Eq. [6], and the only difference is the choice of the prior term.

MAP offers flexibility and robustness regarding noise modelling. Assuming that the noise follows a Gaussian distribution and that the error between frames is independent, the MAP becomes similar to the deterministic regularization scheme if the same regularizer is used. If the prior constraint is a convex function, the MAP process converges toward a unique solution when, for example, a gradient descent algorithm is applied on Eq. [12].

Projection Onto Convex Sets. Incorporating a priori knowledge into the solution can be interpreted as restricting the solution to be a member of a closed convex set C_i that is defined as a set of vectors which satisfies a particular property (47). If the constraint sets have a nonempty intersection, then a solution that belongs to the intersection set: $C_s = \cap_{i-1}^N C_i$, which is also a convex set, can be found by iteratively alternating projections onto these convex sets. The central theorem of projection onto convex sets (POCS) is as follows:

$$X^{(k+1)} = P_m P_{m-1} \ldots P_2 P_1 X^{(k)} \qquad [13]$$

where $X^{(0)}$ is an arbitrary starting point that converges weakly to a feasible solution that lies in C_s. The central problem in POCS is to synthesize the projectors $P_i (i = 1, \ldots, m)$ that project an arbitrary signal X onto the closed, convex sets, C_i. As stated in Ref. *48* and resumed in Ref. *34*, and based on the observation model of Eq. [3], a constraint set is represented by:

$$C_i = \{X : |e^{(X)}| \le \delta_0\} \qquad [14]$$

where $e^{(X)} = Y_k - W_k \hat{X}$ is the model error, and δ_0 is a bound reflecting the statistical confidence, with which the actual image is a member of the set C_i. The projection of an arbitrary image onto C_i can be defined as:

$$\hat{X}^{n+1} = \begin{cases} \hat{X}^n + \frac{(e^{(\hat{X})} - \delta_k) W_k}{\sum_{p,q} W_k^2(p,q)}, & \text{if } e^{(\hat{X})} > \delta_k \\ \hat{X}^n, & \text{if } |e^{(\hat{X})}| \le \delta_k \qquad [15] \\ \hat{X}^n + \frac{(e^{(\hat{X})} + \delta_k) W_k}{\sum_{p,q} W_k^2(p,q)}, & \text{if } e^{(\hat{X})} < -\delta_k \end{cases}$$

Generally, POCS method gives better results, when the data is noisy, dynamic, inconsistent, and/or overdetermined, because it relies on strong spatial domain assumptions. It has been quite extensively used in the MRI context (*23, 49–51*). POCS has been coupled with wavelet coefficient estimation in Ref. *27* and showed to be efficient when applied on temporal sequences. In Ref. *52*, POCS has been used in a frequency based SR algorithm in the context of PROPELLER data fusion. According to Ref. *34*, these methods have the disadvantages of nonuniqueness of solution, slow convergence, and high computational cost.

Choice of SR Method

The goal of this section is to aid the reader to choose the method that fits his problem. Up to now, few studies have been done to compare the performance SR methods. Plenge et al. (*12*) quantitatively and qualitatively compare isotropic reconstructions obtained six

Table 1 Summary of the Presented Methods.

	IBP	Regul-SR	MAP	POCS
Convergence speed	+	+	+	−
Uniqueness of solution	−	+	+	−
Inclusion of spatial priors	−	+	+	+
Noise modeling	−	−	+	+

different SR methods based on IBP, algebraic reconstruction, and regularized approaches. The resulting high-resolution volumes are compared to a reference volume, which was directly acquired at the same isotropic resolution. Resolution metrics as well as SNR values are used to asses the quality of the reconstructed volumes of phantom and real data. All tested SR approaches were able to reconstruct volumes with significantly higher SNR the volume directly acquired at high resolution for a fixed acquisition time, but no particular method significantly outperformed the others. It was also pointed out in this study that the performance of each SR method depends on the nature of the data on which it is applied, making it hard to establish a robust and realistic ranking of the different algorithms. Following this statement, it would be of great utility to study the robustness of each algorithm to various artifacts that usually corrupt real data (acquisition noise, motion blur, and registration errors) to choose the SR algorithm in accordance with the nature and particularities of the data. But to our knowledge, no such studies have been performed to date in the context of MRI.

Generally speaking, each SR algorithm has specific characteristics that can help the user choose the one that fits his data. Each situation has particular constraints (computational time limitations, prior knowledge about the desired solution, prior knowledge about the noise) that can lead the user to favor one algorithms instead of others. We summarize in Table 1 some properties of the different SR algorithms that have been presented in this article. It can be seen from Table 1 that if no prior information is available on the noise characteristics, and if the widely used Gaussian model is admitted for the MAP formulation, the MAP and Regul-SR formulations will lead to similar performance, if the same regularizer is used. In this situation, the choice of the model parameters (PSF and geometric deformation) will have a much greater impact on the result than the choice of the algorithm itself. Unlike Regul-SR, MAP and POCS can model new noise priors, and POCS becomes an interesting alternative if the computational time is not an issue. Also note that the uniqueness of solution for both Regul-SR and MAP is valid only in the
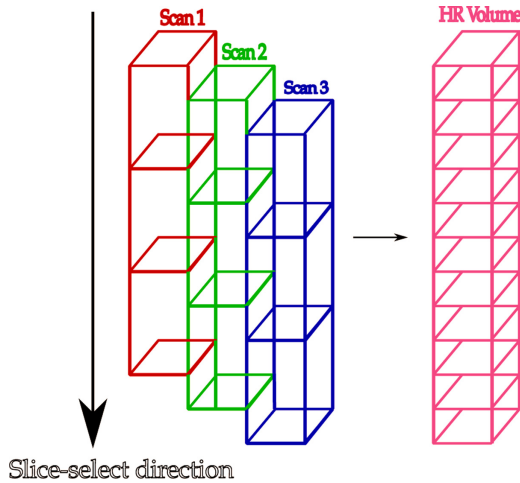
Figure 5   Three shifted parallel scans in the through-plane direction.

case where convex regularizers are used. However, this is not guaranteed for the POCS and IBP approaches that can be problematic in terms of result reproducibility.

Finally, it is important to note that the choice of the minimization method will also influence the speed of the SR process and even sometimes the solution itself (*53*). Although the steepest gradient descent algorithm is widely used because of its simplicity, other methods including, but not restricted to, the conjugate gradients (*54*) and preconditioned gradients (*55*) can also be applied to solve the SR problem and can improve the overall convergence rate.

IV. SR OF STATIC SUBJECTS

The first applications of SR on MRI were performed on static subjects. Because SR requires different views

from the same scene to add new information, movements have to be created artificially by changing the scan FOV or by manually shifting the subject itself. These approaches have been used to increase both in-plane and through-plane resolutions multislice MRI. In Section II, difficulties and limitations of in-plane resolution improvement have been described. Therefore, this section only addresses different protocols that have been suggested to enhance the through-plane resolution of multislice MRI scans.

Parallel Stacks Acquisition

In the early stages of SR applied to MRI, an innovative approach was proposed in Ref. *19*. It consists of acquiring several sets of multislice scans, shifted in the through-plane dimension by a known subpixel distance. The different sets are then combined using a SR reconstruction algorithm to create one high-resolution multislice set with isotropic voxel size. Figure 5 illustrates the shifted acquisition model for three low-resolution scans. Various applications of parallel scans SR reconstruction can be found in Refs. *25*, *22*, *56*, *39*, and *26*.

To reach isotropic reconstruction, this approach requires a minimum N low-resolution scans with $N = \frac{R_t}{R_i}$, where R_t and R_i are, respectively, the through-plane and in-plane resolutions. If the ratio between R_t and R_i is large, the total acquisition time of N scans can become prohibitive in practice. A high-resolution isotropic reconstruction using parallel scans is presented in axial view in Fig. 6(b), originally from the work of Shilling et al. (*56*). It clearly shows that the parallel scan reconstruction contains more details than the isotropic reconstruction obtained from a single scan that is interpolated in the slice-selection dimension shown in Fig. 6(a). The original scan resolution was
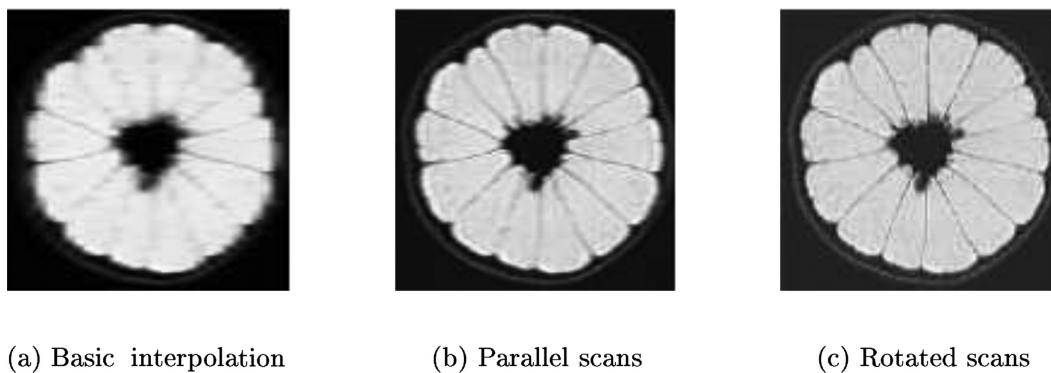

(a) Basic interpolation   (b) Parallel scans   (c) Rotated scans

Figure 6   Comparison of three isotropic reconstructions. Slice-select direction is from left to right. a: Basic interpolation; b: parallel scans; and c: Rotated scans. (From Shilling et al., IEEE International Conference on Image Processing, 2008, 2240–2243, ©IEEE, reproduction by permission.)
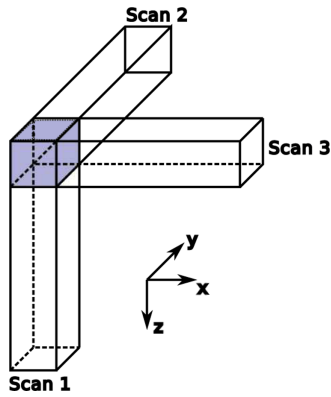
Figure 7 Example of three voxels obtained with orthogonal scans. Each voxel is elongated in the slice-select direction.

$0.6 \times 0.6 \times 3.6 \, \text{mm}^3$, and the slice shift increments were 0.6 mm between each scan. Six low-resolution scans were acquired to reach isotropic reconstruction, that is, $0.6 \times 0.6 \times 0.6 \, \text{mm}^3$.

Multi-Orientation Scans

Multiorientation scan combination has been studied for a long time notably in the context of cardiac imaging (*57, 58*) but has only recently been addressed under a SR framework. Like parallel scan reconstruction, it aims at creating isotropic voxels from several anisotropic scans. However, the acquisition planes are rotated in the frequency and/or phase encoding directions instead of being shifted, resulting in a more efficient sampling of the *k*-space. Theoretically, only two orthogonal stacks are required to ensure isotropic reconstruction. In the case of parallel stack reconstruction, the number of scans required depends on the through-plane to in-plane resolution ratio. Consequently, combinations of multiorientation scans offers a better trade-off regarding acquisition time versus resolution enhancement. An illustration of the combination of orthogonal scans is presented in Fig. 7. It can be seen that each volume has only one low-resolution axe (in the slice-select direction), which is compensated by the acquisition of the other volumes. Applications of such combinations can be found in Refs. *33, 29*.

Following the same concept, an alternative combination of volume consists of rotating the acquisition plane around one commonly encoded axis (*50, 51*) as illustrated in Fig. 8. However, this approach requires the acquisition of more than two scans to ensure a sufficient sampling of the *k*-space and to allow isotropic reconstruction. But if scanning time is not an issue, a sufficient number of volumes can be acquired and combined to reconstruct an isotropic volume. For

example, Poot et al. (*32*) have combined up to 36 volumes to reconstruct a high-resolution isotropic volume. The optimal number of combined low-resolution images has been discussed in Ref. *59* in the context of 2D SR and in Ref. *12* in the context of MRI. Both studies show that the resolution is improved until a certain number of low-resolution images is reached, suggesting that it is not always a good strategy to increase the low-resolution input number. So far, no theoretical bound has been found, and the optimal number of low-resolution inputs is still application dependent.

Both parallel and rotated scans approaches have shown to perform well to add information in the slice-select direction. Orthogonal scan combination has the advantage of minimizing the redundancy between each acquired volumes, which is particularly useful when only a limited number of volumes can be acquired. An example of the superiority of rotated scans versus parallel scans is shown in Fig. 6c. The same number of scans are used for parallel scan and rotated scan combination. The angle increment between rotated scans is 30°. Shilling et al. (*56*) have discussed the advantages of multiorientation scans compared to parallel scans in (*56*). They showed using various metrics that spatial frequencies are better retrieved, when multiorientation stacks are used. The combination of multiorientation shows a better ability to attenuate the partial volume effect that occurs in the slice-select dimension. This is verified by visual inspection of Fig. 6 that clearly shows an improvement in terms of sharpness and detail recovery, when rotated scans are used.
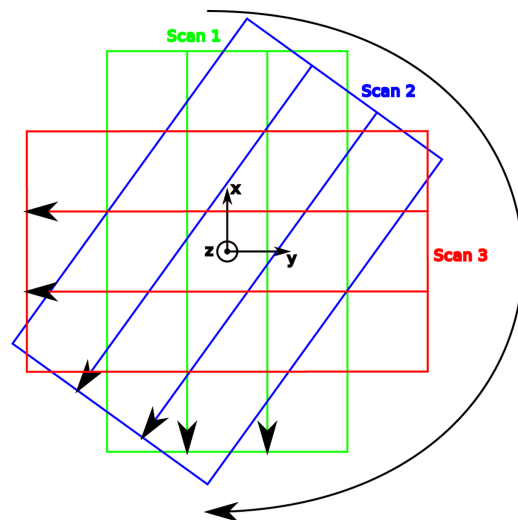

Figure 8 Example of three rotated scans with a common encoded axis (*z*).

V. SR ON MOVING SUBJECTS

To perform SR on static subjects, motion is artificially created by shifting or rotating the scanning plane by a known value. This section studies the application of SR methods for moving subjects where motion comes from the subject itself and is, therefore, not controlled. Two types of motion can be identified, namely, rigid and deformable motion. So far, mostly rigid motion have been studied, but recently a few applications on deformable motion have also been reported.

Rigid Motion

Rigid motion typically occurs when the scanned subject cannot remain still during imaging. This is notably the case for awake neonates, involuntary moving adult subjects, and fetuses. To avoid motion artifacts, acquisition times must be kept as short as possible. This often results in a general decrease in the in-plane resolution and an increase in slice thickness (voxel anisotropy). Consequently, the need for postacquisition resolution enhancement techniques is of great importance in the presence of motion. Motion estimation via registration methods becomes a key step in the SR process and is a major factor influencing the quality of the reconstruction. This section reviews different approaches that have been suggested to apply SR on moving subjects with rigid motion.

In-Plane Resolution Improvement. Hsu et al. (*27*) applied SR on a 2D sequence of cardiac images to improve the in-plane resolution. In the presence of motion, in-plane resolution enhancement is possible, as motion ensures that two consecutive acquisitions contain distinct information about the subject (refer to Section II for in-plane resolution improvement issues). They ignored the deformable nature of the heart and performed affine registration to compute the motion among three successive frames. The SR results presented sharpness improvement when compared to a cubic-spline interpolation.

Another in-plane resolution enhancement method using SR methods based on PROPELLER acquisition has been studied in Ref. *52* based on the work of Pipe (*60*). It consists of registering partial *k*-space acquisitions of different orientations and fusion of the registered images into a high-resolution reconstruction. It has not been, to our knowledge, extended to 3D MRI volumes and slice thickness reduction.

Through-Plane Improvement. 3D representation via 2D multislice acquisition is an issue in the presence of motion, as two consecutive slices can be nonconsistent when looking at the orthogonal planes, as shown in Figs. 9(a–c). Different MRI acquisition protocols have been suggested to handle interslice inconsistency due to motion.

Jiang et al. (*61*) used single-slice snapshot imaging to freeze the motion of fetal subjects. Sequential shifted acquisition was performed to cover the entire subject and ensure a sufficient sampling density. Retrospective alignment of slices inside the volume was performed using a six degree-of-freedom rigid registration and referred as slice-to-volume alignment. Then, a data fusion algorithm based on B-spline scattered data interpolation (SDI) was applied to produce a self-consistent 3D volume of fetal brains. The same authors have also applied this concept to increase the resolution of diffusion tensor images of inutero fetal brain data in Ref. *62*.

Rousseau et al. (*63*) had previously proposed a similar method. The acquisition procedure was, however, different, as they acquired three orthogonal volumes as detailed in Section "Multiorientation Scans". Slice-to-volume registration was applied independently for each volume. The three volumes were then registered to each other before applying the reconstruction algorithm to obtain the high-resolution volume. A similar method was detailed in Ref. *64*. An interesting optimization of the slice-to-volume registration algorithm has been proposed in Ref. (*65*) to avoid the time consuming systematic registration of every 2D slice.

A mathematical framework that justifies the optimality of the reconstructed volume given the acquired MRI data has been developed by Gholipour et al. (*43*). The same authors have proved the superiority of a SR MAP approach compared to a standard SDI in Ref. *29*. An example of reconstruction of a high-resolution volume of a fetal brain from the work of Gholipour et al. is presented in Fig. 9. Slice thickness is set at 6 mm to keep short scanning times and avoid motion artifacts and to preserve a correct SNR. Three orthogonal planes were acquired, for a total number of 60 slices, and combined to produce the high-resolution output. The reconstructed volume reflects the continuity of the brain anatomy in all three planes. Such continuity could not be observed in the acquired volumes, because they were corrupted by partial volume effect, large slice thickness, and motion artifacts. The SR result was shown to be superior in terms of sharpness than the standard SDI, when the same number of input slices were used.

Recently, Super-Resolution Reconstruction (SRR) was applied on diffusion weighted imaging in Ref. *13*. They acquired three 3D orthogonal volumes at a resolution of $1.25 \times 1.25 \times 2.5$ mm^3 and addressed the

(a) Original (Axial) (b) Original (Coronal) (c) Original (Sagittal)

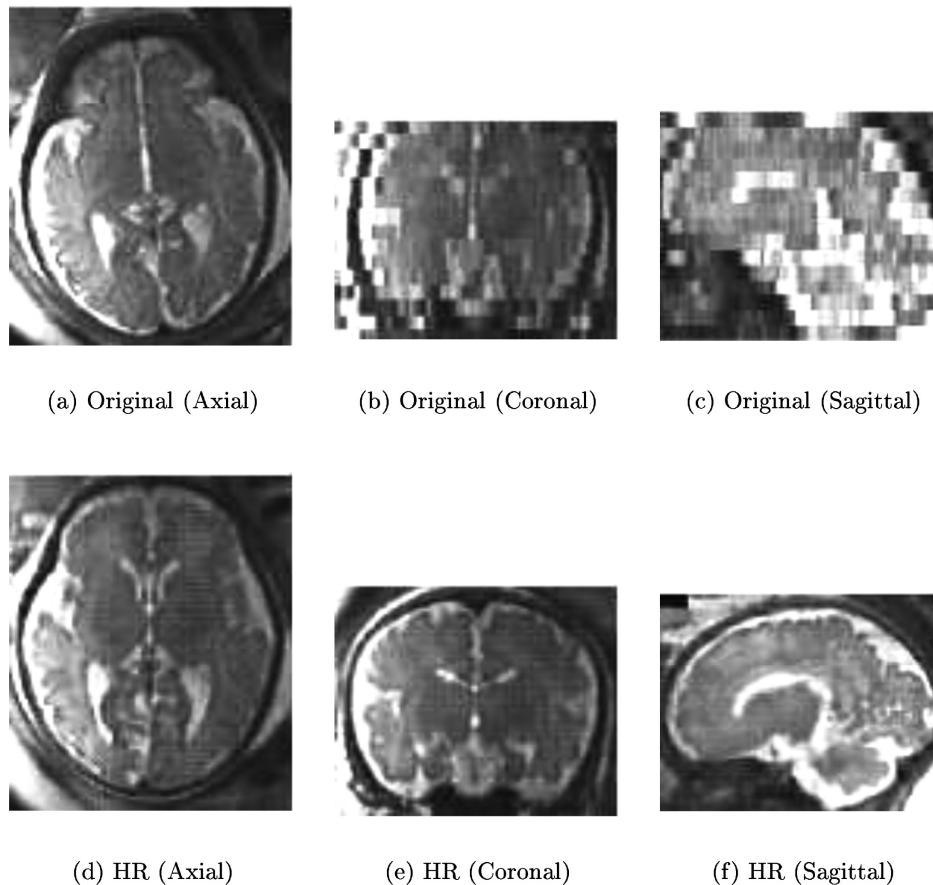(d) HR (Axial) (e) HR (Coronal) (f) HR (Sagittal)

Figure 9 Illustration of motion artifacts when the slice is acquired in the axial plane (a–c). The high-resolution (HR) volume obtained after slice-to-volume registration and SR reconstruction is shown in (d–f). Orginal (a: axial; b: coronal; and c: sagittal) and HR (d: axial; e: coronal; and f: sagittal). (From Gholipour et al. IEEE Trans Med Imaging, 2010, 29, 1739–1758, ©IEEE, reproduction by permission.)

problem of patient motion by aligning the volumes in both space and q-space. Distortion during acquisition was considered and combined with a MAP SR framework to produce an isotropic output volume of resolution $1.25 \times 1.25 \times 1.25$ mm^3. Interestingly, the reconstructed volume presented higher SNR than the volume directly acquired at the same isotropic resolution with an equivalent acquisition time.

Deformable Motion

SR has seldom been applied to subjects that present deformable motion. The main reason for this is the difficulty for deformable registration methods to guarantee sub-pixel accuracy. However, Rahman et al. have applied SR in the context of cardiac imaging to improve the resolution of the left ventricle in (*44*) and (*46*) which deforms with time. More recently, Woo et al. have focused on improving the resolution of tongue MRI

data in (*66*). In both studies, isotropic reconstruction was considered.

In the work of Rahman et al., each slice had to be acquired with coarse resolutions because of the high-frequency heart beats ($1.5 \times 1.5 \times 8$ mm^3) using a gated acquisition technique to synchronize the slice acquisition at the same phase of the cardiac cycle. Three orthogonal scans were acquired using a non-specified sequence. A deformable registration algorithm using the Demons algorithm described in (*67*) was first performed to match the several orthogonal acquisitions. The registered volumes were then fused using a SR MAP algorithm to produce the isotropic volume. The effects of using rigid registration instead of deformable registration were studied and showed that despite the registration errors, the deformable registration algorithm still produced superior quality reconstruction. The authors also compared the effect of using either two or three orthogonal volumes for SR reconstruction. Interestingly, using three volumes degraded the output

volume quality. According to the authors, the additional information brought by the third volume was masked by the accumulation of registration errors.

The article focusing on tongue data presented different characteristics because the scanned subjects could remain still for 1.5 to 3 minutes in order to acquire volumes at a significantly higher resolution of $0.94 \times 0.94 \times 3$ mm^3. Rigid registration followed by a local deformable registration using the Demons algorithm as well as histogram matching were performed to fit the three orthogonal volumes in the same sampling space. The isotropic result obtained with a MAP SR method using a Markov random field based regularizer showed convincing detail enhancement.

Comparing these two studies emphasizes the critical role of registration in the SR process. It suggests that deformable registration is not always able to deliver accurate sub-pixel motion information. The performance of deformable registration is likely to differ with regards to the input volume resolution, the nature and amplitude of the motion, or the ratio between in-plane and through-plane resolutions. The registration inability to accurately estimate the subject deformation in some situations is a current limitation to the applicability of SR on deformable subjects.

VI. MEASURING THE RESOLUTION IMPROVEMENT

It is clearly a real challenge to measure quantitatively the resolution enhancement of SR applied on real MRI images, because in most cases the high-resolution reference image is not available. Visual inspection is widely used when obvious details are added by the SR method. Evaluation by doctors is also a precious input to judge the benefit of proposed approaches. However, this does not allow the performance of different methods to be objectively quantified and is not convenient when large datasets must be evaluated. Unfortunately, there are no standard procedures to measure or compare the resolution of reconstructed SR images. In addition, the performance of SR algorithms is highly dependent on the data on which it is applied. This part reviews some quantitative evaluation methods that have been used in the literature, which could form a starting point for a further common resolution evaluation procedure.

Sigmoid Fitting

This technique aims at measuring the edge width, or transition width, using a least-square fitting to a sigmoid function of the form:

$$s(x) = \frac{1}{1 + \exp(-a(x - c))} \qquad [16]$$

The parameter a is inversely proportional to the edge width, and c corresponds to the edge centre location. Once the optimal curve fitting is obtained, a measure of rise length is computed and defined as the width from 10 to 90% of the edge height. It is easily shown that the edge width in pixels is defined by:

$$\text{width} = \frac{4.4}{a} \qquad [17]$$

A significant drop in the edge width can be interpreted as a gain in resolution, as object borders are spread over a lower number of pixels, which makes them easier to resolve. Sigmoid fitting has been used to measure resolution improvement in the following works: Refs. *25*, *36*, and *39*. However, it can be noted that the sigmoid fitting measure is sensible to some edge artifacts such as overshoots as shown in Ref. *12*. This suggests that this approach cannot be used alone as a measure of spatial resolution.

Metrics

Most objective metrics that can be found in the literature require a reference image to compute the error between the reference image and the SR result. This limits the use of metrics as a performance evaluation tool, because the high-resolution reference image is seldom available in clinical studies. Even when a reference image is available, metrics still need to be handled with care. MRI presents inhomogeneity in the contrast and pixel intensities produced, which makes it delicate to apply intensity based metrics such as PSNR, or mean absolute error. To avoid this problem, Gholipour et al. (*43*) have suggested the use of mutual information to compare their reconstructed volume with the high-resolution reference.

Validation Using Further Application

An interesting way to validate the detail improvement is to show the benefit of applying SR on a quantifiable application. Yeshurun et al. (*16*) have improved fiber tract mapping using SR. Other articles have demonstrated the improvement of segmentation results using SR in Refs. *37* and *46*. Metrics such as the Dice similarity coefficient can be computed to evaluate the SR-based segmentation based on a manual reference segmentation.

Phantoms

The main advantage of using phantoms is the possibility to control the characteristics of the scanned subject, providing a ground truth reference toward which the SR reconstruction should converge. In the context of isotropic reconstruction, isotropic high-resolution scans are often performed and compared to the isotropic reconstruction obtained from anisotropic sets. Phantoms are often used as a proof of concept for the proposed method, but they do not ensure the validity of the observed resolution improvement when the algorithm is applied on real data. Resolution improvement shown using phantom data is a necessary condition, but not sufficient, to conclude on a resolution gain on real MRI data. Phantoms have been used to compare and measure the performances of different SR algorithms in Refs. *12* and *68*.

Several phantoms have been proposed to prove and quantify an eventual resolution gain. Greenspan et al. (*36*) have proposed a comb-like phantom that presents equally spaced teeth in the slice-select direction that is enhanced by the proposed SR algorithm. Carmi et al. (*22*) suggested a similar set-up in but with different known spacing between the plastic frames to quantify more precisely the resolution gain. Mayer and Virseay (*21*) designed a phantom composed of an orthogonal plastic grid, to measure the feasibility of in-plane resolution improvement. Finally, an experimental procedure for 3D PSF estimation has been developed in Ref. *31* and can be used to evaluate SR algorithm performances using the PSF estimation as a resolution reference measure.

Simulation-Based Evaluation

Realistic physical phantoms representing real organs can be very challenging to build. This is the reason why MRI-simulated phantom have been developed. The BrainWeb simulated database described in Refs. *69*, *70*, *71*, is one of them. This database contains realistic 3D MRI brain data based on real scans, according to user-generated simulated MRI acquisition parameters including slice thickness, FOV, receiver bandwidth, number of signal averages, scan matrix size, pulse sequence (SE, IR, FLASH, spoiled FLASH, FISP, and CE-FAST/PSIF), and pulse sequence parameters (TR, TE, and flip angle). The chosen parameters realistically affect the image properties such as contrast, noise, and partial volume effect. The control one has over these parameters facilitates the development and the accurate evaluation of various postprocessing algorithms like SR, denoising, and segmentation. In the context of SR, high-resolution images can be generated and used as a reference and compared to the reconstructed SR results. Several authors have used this tool to evaluate their algorithm performance, for example, in Ref. *39* and *45*. Finally, as simulated data are fully reproducible by any user, the performance of different image processing algorithms can be objectively compared. However, the validity of a model-based comparison is only as good as the model is close to real data.

VII. CONCLUSIONS AND PERSPECTIVES

This article has covered the possibility to use SR techniques in the context of 2D and 3D MRI data. The dimensionality and feasibility of the problem have been addressed in Section II. It showed that in-plane resolution improvement is possible under certain circumstances, although the resolution gain is limited due to the inherent signal band limitation. SR was shown to be far more efficient when applied in the through-plane direction to reduce voxel anisotropy where aliasing was more likely to appear. The interest of SR in MRI lies in the fact that such spatial resolutions and such SNR could not be reached with a single 3D acquisition. Typically, SR is useful in situations where the acquired resolution is not sufficient to correctly characterize small but clinically significant structures (joints, tumors, pelvis, or brain structures). For example, the spatial resolution of images produced by low spatial resolution sequences such as diffusion weighted imaging have been successfully enhanced.

The main SR algorithms that have been used on MRI data and their respective specificities were presented. Despite the fact that the choice of the SR method is highly dependant on the application, a brief summary of their advantages was given. Then, different acquisition protocols that were applied on static subjects were discussed. It was shown that better reconstruction was obtained when multiorientation scans rather than parallel scans were combined. SR results have been compared to linear interpolation methods such as zero-padding interpolation, cubic-spline, or SDI. Edge sharpness superiority and detail addition were observed in the SR results that were confirmed by several objective metrics.

In the presence of motion, registration becomes a key step in the SR procedure. Successful SR reconstruction was obtained in the case of rigid motion, but the performances on deformable subjects were not always as successful due to the accumulation of registration errors. Deformable registration accuracy is a current limitation to the success of SR methods in this context. Finally, several ways of measuring the resolution gain are summarized in Section VI and can

be considered as an essential complement to visual inspection. As a conclusion, this section covers several aspects of SR applied to MRI that in our view present interesting perspectives.

Evaluation of SR Algorithm Robustness

SR algorithm comparisons have been done in Ref. *12* on phantom and real data. No particular method outperformed the others in terms of both resolution enhancement and SNR improvement, and the authors pointed out the performance of each method was highly application dependent. A useful complementary study could consist of evaluating the robustness of each algorithm to various artifacts that usually corrupt real MRI data (acquisition noise, motion blur, and registration errors) to facilitate the choice of the SR algorithm in accordance with the nature and particularities of the data. As SR results are particularly sensitive to registration errors, it could be interesting to study the development of algorithms that take into account motion estimation errors. To our knowledge, no such studies have been performed so far in the context of volumetric MRI data and could be of great use.

Temporal Resolution Improvement

While the temporal aspect of SR has been extensively studied and successfully applied in video applications, it has seldom been addressed in the context of MRI. Temporal resolution improvement could be useful to have a better understanding of dynamic phenomena. For example, it could improve the tracking of moving organs such as moving structures of the heart, upper abdominal visceral organs like the liver, or moving tumors to optimize radiotherapy treatment. The addition of the temporal dimension would not affect the SR framework, as it has been established so far, but the increasing computational complexity of the problem would have to be handled.

Explicit Registration Methods

The inability to guarantee perfect registration is clearly a bottleneck for the application of SR algorithms. To overcome this issue, methods of SR without explicit motion estimation have recently been studied in Refs. *72* and *73* and showed promising results to improve the resolution of video sequences. They implicitly used the motion information to reconstruct high temporal and spatial resolution image sequences with improved SNR. Using this approach might reduce the registration errors impact on the high-resolution MRI volumes. However, the dramatic increase in the computational cost that will occur when the method is extended to 3D MRI scans might be challenging to overcome. The extension of this method to volumetric MRI data of subjects presenting deformable motion remains to be explored.

Optimization of SR Parameters

In the context of 3D isotropic reconstruction, the influence of various SR parameters have been studied. Plenge et al. (*12*) have studied the evolution of the resolution enhancement and SNR improvement when the number of low-resolution inputs is increased. The authors showed that SR performance does not necessarily increase when more low-resolution scans are added and could even decrease in some cases. Although no theoretical bound has been determined so far, similar trends are likely to be observed in other situations. Other SR parameters have not been evaluated and could benefit from further investigation. One particular parameter that has not been studied in the context of isotropic SR reconstruction is the optimal ratio between through-plane and in-plane resolutions for a given voxel volume (or a fixed acquisition time). On one hand, highly anisotropic voxels introduce partial volume effect that might degrade the overall SR performance. On the other hand, more isotropic voxels might limit the potential resolution enhancement. Finding the optimal voxel anisotropy would ensure to reach the optimal resolution enhancement, when the high-resolution volume is reconstructed.

Resolution Enhancement Limits

In 2D, limits of SR in terms of resolution improvement have been studied by Lin and Shum (*59*) for both practical and synthetic situations. They stated that in the case of translational motion, the resolution improvement limit was 1.6 for real data and 5.7 for synthetic data (note that these results have been discussed in Refs. *74* and *75*). They also mention that these theoretical limits might increase in the presence of other types of motion. Following this idea, Robinson and Milanfar (*76*) stated that a single bound cannot be generalized for any SR scenario. The resolution improvement limit was shown to be a complex relationship between measurement SNR, number of observations, nature of the motion, image content, and the imaging system PSF. The authors particularly pointed out the performance superiority in the case of known motion compared to the case of estimated motion. Generally, the more a priori information is incorporated into the problem, the better the resolution improvement. Such studies have only been performed for rigid motion of 2D images

only, so theoretical limits still have to be determined for volumetric data and for various types of motion. In practice, such a limit would help to determine the size of anatomical structures that could possibly be resolved using SR approaches, depending on the resolution of the acquired low-resolution scans.

ACKNOWLEDGMENT

REFERENCES

1. Liu L, Liang S, Li L, Mao Y, Tang L, Tian L, et al. 2009. Prognostic impact of magnetic resonance imaging-detected cranial nerve involvement in nasopharyngeal carcinoma. Cancer 115:1995–2003.

2. van der Heide UA, Houweling AC, Groenendaal G, Beets-Tan RG, Lambin P. 2012. Functional MRI for radiotherapy dose painting. Magn Reson Imaging 30:1216–1223.

3. Buchbender C, Heusner TA, Lauenstein TC, Bockisch A, Antoch G. 2012. Oncologic pet/MRI, part 1: Tumors of the brain, head and neck, chest, abdomen, and pelvis. J Nucl Med 53:928–938.

4. Chavhan GB, Babyn PS. 2011. Whole-body MR imaging in children: principles, technique, current applications, and future directions. Radiographics 31:1757–1772.

5. Webb A. 2003. Introduction to Biomedical Imaging. In: IEEE Press Series in biomedical engineering, New York: Wiley-Interscience.

6. Regatte RR, Schweitzer ME. 2007. Ultra-high-field MRI of the musculoskeletal system at 7.0t. J Magn Reson Imaging 25:262–269.

7. Moats RA, Sendhil Velan S, Jacobs R, Gonzalez-Gomez I, Dubowitz DJ, Taga T, et al. 2003. Micro-MRI at 11.7 t of a murine brain tumor model using delayed contrast enhancement. Mol Imaging 2:150–158.

8. Tsai R, Huang T. 1980. Moving image restoration and registration. In: IEEE International Conference on Acoustics, Speech, and Signal Processing, Denver, CO April 9–11, 1980, Vol. 5. pp 418–421.

9. Irani M, Peleg S. 1990. Super resolution from image sequences. In: International Conference on Pattern Recognition, Atlantic City, USA, Vol. 2. pp 115–120.

10. Kim S, Bose N, Valenzuela H. 1990. Recursive reconstruction of high resolution image from noisy undersampled multiframes. IEEE Trans Acoust Speech 38:1013–1027.

11. Irani M, Peleg S. 1991. Improving resolution by image registration. Graph Models Image Process 53:231–239.

12. Plenge E, Poot DHJ, Bernsen M, Kotek G, Houston G, Wielopolski P, et al. 2012. Super-resolution reconstruction in MRI: better images faster? In: Haynor DR, Ourselin S, eds., SPIE Medical Imaging, Vol. 8314. Bellingham, WA: SPIE Press, P83143V.

13. Scherrer B, Gholipour A, Warfield SK. 2012. Super-resolution reconstruction to increase the spatial resolution of diffusion weighted images from orthogonal anisotropic acquisitions. Med Image Anal 16:1465–1476.

14. Fiat D. 1997. Method of enhancing an MRI signal. Number U.S. Patent 6,294,914.

15. Greenspan H. 2009. Super-resolution in medical imaging. Comput J 52:43–63.

16. Yeshurun Y, Peled S. 2001.Superresolution in MRI: application to human white matter fiber tract visualization by diffusion tensor imaging. Magn Reson Med 45:29–35.

17. Tieng QM, Cowin GJ, Reutens DC, Galloway GJ, Vegh V. 2011. MRI resolution enhancement: how useful are shifted images obtained by changing the demodulation frequency? Magn Reson Med 65:664–672.

18. Scheffler K. 2002. Superresolution in MRI? Magn Reson Med 48:408–408.

19. Greenspan H, Oz G, Kiryati N, Peled S. 2002. MRI inter-slice reconstruction using super-resolution. Magn Reson Imaging 20:437–446.

20. Uecker M, Sumpf TJ, Frahm J. 2011. Reply to: MRI resolution enhancement: how useful are shifted images obtained by changing the demodulation frequency? Magn Reson Med 66:1511–1512.

21. Mayer GS, Vrscay ER. 2007. Measuring information gain for frequency-encoded super-resolution MRI. Magn Reson Imaging 25:1058–1069.

22. Carmi E, Liu S, Alon N, Fiat A, Fiat D. 2006. Resolution enhancement in MRI. Magn Reson Imaging 24:133–154.

23. Lu Y, Yang R, Zhang J, Zhang C. 2010. Super resolution image reconstruction in parallel magnic resonance imaging. In: 8th IEEE International Conference on Control and Automation, Xiamen, China, June 9–11, 2010. pp 761–766.

24. Elad M, Feuer A. 1997. Restoration of a single super-resolution image from several blurred, noisy, and under-sampled measured images. IEEE Trans Image Process 6:1646–1658.

25. Peeters RR, Kornprobst P, Nikolova M, Sunaert S, Vieville T, Malandain G, et al. 2004. The use of super-resolution techniques to reduce slice thickness in functional MRI. Int J Imaging Syst Technol 14:131–138.

26. Ziye Y, Yao L. 2009. Super resolution of MRI using improved ibp. In: International Conference on Computational Intelligence and Security, London, England August 26–28, 2009. Vol. 1. pp 643–647.

27. Hsu JT, Yen CC, Li CC, Sun M, Tian B, Kaygusuz M. 2004. Application of wavelet-based pocs super-resolution for cardiovascular MRI image enhancement. In: Third International Conference on Image and Graphics, Hong Kong, China, December 18–20, 2004. pp 572–575.

28. Joshi S, Marquina A, Osher S, Dinov I, Van Horn J, Toga A. 2009. Edge-enhanced image reconstruction using (TV) total variation and bregman refinement. In: Scale

Space and Variational Methods in Computer Vision, Vol. 5567. Berlin/Heidelberg: Springer. pp 389–400.

29. Gholipour A, Estroff J, Sahin M, Prabhu S, Warfield S. 2010. Maximum a posteriori estimation of isotropic high-resolution volumetric MRI from orthogonal thick-slice scans. In: MICCAI, Beijing, China, September 20–24, 2010, Vol. 6362. Berlin/Heidelberg: Springer. pp 109–116.

30. Gholipour A, Polak M, van der Kouwe A, Nevo E, Warfield SK. 2011. Motion-robust MRI through real-time motion tracking and retrospective super-resolution volume reconstruction. In: International Conference of the IEEE Engineering in Medicine and Biology Society, Boston, MA, USA, August 30–September 3, 2011. pp 5722–5725.

31. Moon SY, Hornak JP. 2010. A volume resolution phantom for MRI. Magn Reson Imaging 28:286–289.

32. Poot D, Van Meir V, Sijbers J. 2010. General and efficient super-resolution method for multi-slice MRI medical image computing and computer-assisted intervention. In: MICCAI, Vol. 6361. Berlin/Heidelberg: Springer. pp 615–622.

33. Souza A, Senn R. 2008. Model-based super-resolution for MRI. Conf Proc IEEE Eng Med Biol Soc 2008:430–434.

34. Park SC, Park MK, Kang MG. 2003. Super-resolution image reconstruction: a technical overview. IEEE Signal Proc Mag 20:21–36.

35. Irani M, Peled S. 1993. Motion analysis for image enhancement: Resolution, occlusion, and transparency. J Vis Commun Image Represent 4:324–335.

36. Greenspan H, Oz G, Kiryati N, Peled S. 2002. Super-resolution in MRI. In: IEEE International Symposium on Biomedical Imaging: Nano to Macro, Washington, DC, USA, July 7–10, 2012. pp 943–946.

37. Joshi SH, Marquina AM, Osher SJ, Dinov I, Van Horn JD, Toga AW. 2009. MRI resolution enhancement using total variation regularization. In: IEEE International Symposium on Biomedical Imaging. pp 161–164.

38. Rudin L, Osher S, Fatemi E. 1992. Nonlinear total variation based noise removal algorithms. Physica D 60:259–268.

39. Ben-Ezra A, Greenspan H, Rubner Y. 2009. Regularized super-resolution of brain MRI. In: IEEE International Symposium on Biomedical Imaging: Nano to Macro, Boston, MA, USA, June 28–July 1, 2009. pp 254–257.

40. Nedjati-Gilani S, Alexander DC, Parker GJM. 2008. Regularized super-resolution for diffusion MRI. In: IEEE International Symposium on Biomedical Imaging. pp 875–878.

41. Rousseau F, Kim K, Studholme C. 2010. A groupwise super-resolution approach: application to brain MRI. In: IEEE International Symposium on Biomedical Imaging: Nano to Macro, Rotterdam, The Netherlands, April 14–17, 2010. pp 860–863.

42. Rousseau F. 2010. A non-local approach for image super-resolution using intermodality priors. Med Image Anal 14:594–605.

43. Gholipour A, Estroff JA, Warfield SK. 2010. Robust super-resolution volume reconstruction from slice acquisitions: application to fetal brain MRI. IEEE Trans Med Imaging 29:1739–1758.

44. Rahman Sur, Wesarg S. 2010. Upsampling of cardiac MR images: Comparison of averaging and super-resolution for the combination of multiple views. In: 10th IEEE International Conference on Information Technology and Applications in Biomedicine (ITAB 2010), Corfu, Greece, November 3–5, 2010. pp 1–4.

45. Bai Y, Han X, Prince JL. 2004. Super-resolution reconstruction of MR brain images. In: Proceedings of the 38th Annual Conference on Information Sciences and Systems (CISS'04), Princeton, NJ, USA, March 2004.

46. Rahman Sur, Wesarg S. 2010. Combining short-axis and long-axis cardiac MR images by applying a super-resolution reconstruction algorithm. In: SPIE Medical Imaging, Image Processing, San Diego, CA, USA, February 2010, Vol. 7623. Bllingham, WA: SPIE Press.

47. Starck H, Oskoui P. 1989. High-resolution image recovery from image-plane arrays, using convex projections. J Opt Soc Am A 6:1715–1726.

48. Tekalp A, Ozkan M, Sezan M. 1992. High-resolution image-reconstruction from lower-resolution image sequences and space-varying image-restoration. In: International Conference On Acoustics, Speech, And Signal Processing (ICASSP 1992), San Francisco, CA, USA, March 23–26, 1992, Vols. 1–5.

49. Pena JG, Toterman S, Park KJ. 2001. MRI isotropic resolution reconstruction from two orthogonal scans. In: SPIE Medical Imaging, Vol. 4322. Bellingham, WA: SPIE Press, pp 87–97.

50. Shilling R, Brummer M, Mewes K. 2006. Merging multiple stacks MRI into a single data volume. In: 3rd IEEE International Symposium on Biomedical Imaging: Nano to Macro, Arlington, VA, USA, April 6–9, 2006, pp 1012–1015.

51. Shilling RZ, Robbie TQ, Bailloeul T, Mewes K, Mersereau RM, Brummer ME. 2009. A super-resolution framework for 3-d high-resolution and high-contrast imaging using 2-d multislice MRI. IEEE Trans Med Imaging 28:633–644.

52. Malczewski KF. 2009. MRI image enhancement by PROPELLER data fusion. Int J Adv Media Commun, 3:25–34.

53. Allwright JC. 1976. Conjugate gradient versus steepest descent. J Optim Theory Appl 20:129–134. DOI:10.1007/BF00933351.

54. Hestenes MR, Stiefel E. 1952. Methods of conjugate gradients for solving linear systems. J Res Nat Bureau Stand 49:409–436.

55. Munksgaard N. 1980. Solving sparse symmetric sets of linear equations by preconditioned conjugate gradients. ACM Trans Math Softw 6:206–219.

56. Shilling RZ, Ramamurthy S, Brummer ME. 2008. Sampling strategies for super-resolution in multi-slice MRI. In: Proceedings of the International Conference on Image

Processing, ICIP 2008, San Diego, CA, USA, October 12–15, 2008. pp 2240–2243.

57. Kuwahara M, Eiho S. 1991. 3-d heart image reconstructed from MRI data. Comput Med Imaging Graph 15:241–246.

58. Goshtasby A, Turner D. 1996. Fusion of short-axis and long-axis cardiac MR images. Comput Med Imaging Graphics, 20:77–87.

59. Lin Z, Shum H. 2004. Fundamental limits of reconstruction-based superresolution algorithms under local translation. IEEE Trans Pattern Anal 26:83–97.

60. Pipe JG. 1999. Motion correction with propeller MRI: application to head motion and free-breathing cardiac imaging. Magn Reson Med 42:963–969.

61. Jiang S, Xue H, Glover A, Rutherford M, Rueckert D, Hajnal JV. 2007. MRI of moving subjects using multislice snapshot images with volume reconstructio (svr): application to fetal, neonatal, and adult brain studies. IEEE Trans Med Imaging 26:967–980.

62. Jiang S, Xue H, Counsell S, Anjari M, Allsop J, Rutherford M, et al. 2009. Diffusion tensor imaging (dti) of the brain in moving subjects: application to in-utero fetal and ex-utero studies. Magn Reson Med 62:645–655.

63. Rousseau F, Glenn O, Iordanova B, Rodriguez-Carranza C, Vigneron D, Barkovich J, et al. 2005. A novel approach to high resolution fetal brain MR imaging. In: 8th International Conference on Medical Image Computing and Computer Assisted Intervention, Palm Springs, CA, USA, October 26–30, 2005. Vol. 3749. Berlin/Heidelberg: Springer. pp 548–555.

64. Rousseau F, Glenn O, Iordanova B, Rodriguez-Carranza C, Vigneron D, Barkovich J, et al. 2006. Registration-based approach for reconstruction of high resolution in utero fetal MR brain images. Acad Radiol 13:1072–1081.

65. Kim K, Habas PA, Rousseau F, Glenn OA, Barkovich AJ, Studholme C. 2010. Intersection based motion correction of multislice MRI for 3-D in utero fetal brain image formation. IEEE Trans Med Imaging 29:146–158.

66. Woo J, Bai Y, Roy S, Murano EZ, Stone M, Prince JL. 2012. Super-resolution reconstruction for tongue MR images. In: Haynor DR, Ourselin S, eds. SPIE Medical Imaging, Vol. 8314. SPIE Press: Bellingham, WA. P83140C.

67. Thirion JP. 1998. Image matching as a diffusion process: an analogy with maxwell's demons. Med Image Anal 2:243–260.

68. Plenge E, Poot DHJ, Bernsen M, Kotek G, Houston G, Wielopolski P, et al. 2012. Super-resolution methods in MRI: can they improve the trade-off between resolution, signal-to-noise ratio, and acquisition time? Magn Reson Med.

69. Kwan RK-S, Evans AC, Pike GB. 1996. An extensible MRI simulator for post-processing evaluation. In: 4th International Conference, VBC '96, Hamburg, Germany, September 22–25, 1996. In: Höhne KH, Kikinis R, eds. Lecture Notes in Computer Science, Vol. 1131. pp 135–140.

70. Kwan RK-S, Evans AC, Pike GB. 1999. MRI simulation-based evaluation of image-processing and classification methods. IEEE Trans Med Imaging 18:1085–1097.

71. Collins D, Zijdenbos A, Kollokian V, Sled J, Kabani N, Holmes C, et al. 1998. Design and construction of a realistic digital brain phantom. IEEE Trans Med Imaging 17:463–468.

72. Protter M, Elad M, Takeda H, Milanfar P. 2009. Generalizing the nonlocal-means to super-resolution reconstruction. IEEE Trans Image Process 18:36–51.

73. Takeda H, Milanfar P, Protter M, Elad M. 2009. Super-resolution without explicit subpixel motion estimation. IEEE Trans Image Process 18:1958–1975.

74. Wang L, Feng J. 2006. Comments on "Fundamental limits of reconstruction-based superresolution algorithms under local translation". IEEE Trans Pattern Anal 28:846.

75. Lin Z, Shum H. 2006. Response to the comments on "Fundamental limits of reconstruction-based superresolution algorithms under local translation". IEEE Trans Pattern Anal 28:847.

76. Robinson D, Milanfar P. 2006. Statistical performance analysis of super-resolution. IEEE Trans Image Process 15:1413–1428.

BIOGRAPHIES

Dr. Eric Van Reeth was born in 1985. He received an engineer degree in Electrical and Electronic Engineering with a major in image processing in 2007, and a Ph.D. degree in collaboration with STMicroelectronics in 2011 from Grenoble INP, France. In 2011, he joined Nanyang Technological University (NTU), Singapore, as a postdoctoral fellow. His current research focuses on resolution enhancement of MRI data.

Dr. Ivan W. K. Tham is an Assistant Professor and consultant radiation oncologist at the National University Cancer Institute, Singapore. He has a special interest in head and neck cancer, lung cancer, and haematological malignancies. Following his undergraduate medical training at the National University of Singapore, he trained in clinical oncology at the National Cancer Centre, Singapore and Guy's and St. Thomas' NHS Foundation Trust, London, UK. His research interests include image-guided intensity modulated radiation therapy, especially in lung and nasopharyngeal cancer. He is also exploring ways to integrate new imaging modalities, such as four-dimensional magnetic resonance imaging to improve treatment accuracy.

Dr. Cher Heng Tan obtained his medical degree from the National University of Singapore in 2001 and completed his training in Diagnostic Radiology in 2009. He is presently a Consultant with the Department of Diagnostic Radiology at Tan Tock Seng Hospital. His subspecialty interests are in oncologic imaging and abdominal MRI, for which he completed a clinical fellowship at MD Anderson Cancer Center, Houston, Texas, USA in 2009. He now serves as Chairman of the Abdominal Radiology Subsection of the Singapore Radiological Society. As a clinical core faculty member of the NHG-AHPL Diagnostic Radiology Residency Program, Cher Heng is involved with training of Radiology residents. He is also a clinical tutor for medical students with Yong Loo Lin School of Medicine (NUS). He is currently involved in a number of funded research projects with various NTU scientists, primarily related to MRI. He has been appointed Specialty Editor for the Singapore Medical Journal.
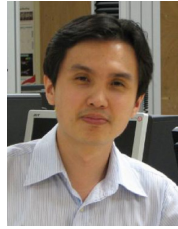
Dr. Chueh Loo Poh is an Assistant Professor with the Division of Bioengineering at Nanyang Technological University (NTU), Singapore since 2007. He obtained his PhD in Bioengineering from Imperial College in 2007 and B.Eng. degree (First class honours class) in Electrical and Electronic Engineering from NTU in 2001. He is a bioengineer whose research focuses on biomedical image processing and analysis, clinical information systems, and computational aspects of synthetic biology.